Jun Zeng · Rui-Qin Zhang
Herbert R. Treutlein *Editors*

Quantum Simulations of Materials and Biological Systems

Springer

Quantum Simulations of Materials and Biological Systems

Jun Zeng • Rui-Qin Zhang • Herbert R. Treutlein
Editors

Quantum Simulations of Materials and Biological Systems

Springer

Editors
Jun Zeng
Qubist Molecular Design Pty. Ltd.
and Monash University
Parkville, Victoria, Australia

Herbert R. Treutlein
Qubist Molecular Design Pty. Ltd.
and Monash University
Parkville, Victoria, Australia

Rui-Qin Zhang
Department of Physics & Material Science
City University of Hong Kong
Hong Kong SAR, People's Republic
of China

ISBN 978-94-007-4947-4 ISBN 978-94-007-4948-1 (eBook)
DOI 10.1007/978-94-007-4948-1
Springer Dordrecht Heidelberg New York London

Library of Congress Control Number: 2012944643

Printed on acid-free paper

Springer is part of Springer Science+Business Media (www.springer.com)

Preface

The 1st International Symposium on Computational Sciences (ISCS2011) took place from April 18 to April 21, 2011 in Shanghai, China. The scientific program of this symposium included many topics related to the methodological development and application of quantum simulations in biology and in the material sciences. The program consisted of plenary and regular presentations and included the following four main themes:

- Recent development of quantum mechanical methods,
- Simulations of biological systems,
- New techniques in material sciences, and
- New techniques in drug design and discovery.

In addition, a workshop on the theory, code and application of DFTB+ method was held on April 21, 2011.

This volume comprises ten chapters written by the selected presenters. These contributions cover three challenging areas in the field of computational sciences: (i) the development and utilization of quantum mechanical methods for improving the accuracy of the system, (ii) the application of computational simulation techniques for investigating the time-scale involved in the processes, and (iii) the generation of more rigorous molecular force fields to solve the problems of systems with significantly large sizes. This book aims to assemble overviews of recent developments as well as some applications of all these three computational techniques. Main focuses of this volume are the methodology and applications of the density functional theory (DFT) method in material sciences and the principles and applications of the combined quantum mechanical molecular mechanical (QM/MM) approach for the biological systems.

One of the key components in DFT theory is the exchange-correlation functionals. Their application in material sciences was reviewed and analyzed by Professor Pietro Cortona in the first chapter. On the other hand, the time-dependent (TD) approach was generally used to calculate the electronic excitations within the DFT frame. In Chap. 2, Professor Thomas Niehaus presents the implementation of the TD algorithm into DFTB+ method to simulate the quantum transportation process

between the metal leads. For the application of the DFT method in large systems such as nanoparticles, Professor Rui-Qin Zhang *et al*. (Chap. 3) used the DFTB+ method to investigate the optical properties of Silicon quantum dots (SQDs) for biological probes and sensors, and Professor Stephan Irle *et al*. described some important QM/MM simulations on the nucleation process of the carbon nanotubes in Chap. 4. In Chap. 5, Professor Zhenyu Li presented how to determine structures and properties of new material such as graphene oxide from a theoretical perspective.

The biological section was firstly highlighted in Chap. 6 by Professor Jeffrey Reimers who describes the recent development on the refinement of X-ray structures of biological system using DFT method. It is followed by Professor Thomas Simonson who in Chap. 7 outlined the current methods available for protein design and engineering and presented a recent application of his design technique for an important family of enzymes. It evokes some possibility of quantum mechanical methods for protein engineering and drug design. The later was discussed by Professor Ying Xue who in Chap. 8 presented their recent works on the ligand-based design of inhibitors of factor Xa using supported vector machine (SVP) method. The DFT method, in the frame of combined QM/MM methodology, has been widely used to quantitatively understand the mechanism of biological processes. In Chap. 9 Professor Dingguo Xu has reviewed some principles and applications of the QM/MM method for the enzyme catalytic mechanism of several biological systems. Finally in Chap. 10, Professor Bo Durbeej brought the application of this method to the excited states by presenting some recent studies in the photochemistry of phytochromes.

We hope that this consolidated volume will give its readers some insights into the recent progresses made in the field of quantum simulations for material and biological systems.

We gratefully acknowledge the financial support received from some industrial sponsors, including SYNthesis Med Chem (Shanghai), and Qubist Molecular Design (Australia) as well as SRD Biosciences Co Ltd (Shanghai). We would also like to thank the Professors Stephan Irle (University Nagoya, Japan), Sanhuang Ke (Tongji University, China) and Dr Balint Aradi (University of Bremen, Germany) for organizing the DFTB+ workshop and Jenny Zeng from SRD Biosciences Co Ltd (Shanghai) for preparing and managing the conference. Finally, we would like to express our sincere thanks to all the participants of ISCS2011 for their support and to all the authors who have contributed with their excellent papers to the realization of this monograph.

College of Chemistry, Sichuan University and
SRD Biosciences Co Ltd (Shanghai), P.R. China — Jun Zeng

Department of Physics and Material Sciences
City University of Hong Kong, Hong Kong, P.R. China — Rui-Qin Zhang

Monash Institute of Pharmaceutical Sciences
and Qubist Molecular Design Pty Ltd, Australia — Herbert R. Treutlein

Contents

Contributors

Carlo Adamo Laboratoire d'Électrochimie, Chimie des Interfaces et Modélisation pour l'Énergie (UMR 7575), Centre National de la Recherche Scientifique, Chimie ParisTech, Paris Cedex 05, France

Duan Chen College of Chemistry, Key Lab of Green Chemistry and Technology in Ministry of Education, Sichuan University, Chengdu, P.R. China

GuanHua Chen Department of Chemistry, The University of Hong Kong, Hong Kong, China

Charles A. Collyer School of Molecular Bioscience, The University of Sydney, Sydney, New South Wales, Australia

Pietro Cortona Laboratoire Structure, Propriétés et Modélisation des Solides, UMR 8580, École Centrale Paris, Châtenay-Malabry, France

Abir De Sarkar Department of Physics and Materials Science, City University Hong Kong, Hong Kong SAR, China

Bo Durbeej Division of Computational Physics, IFM, Linköping University, Linköping, Sweden

Olle Falklöf Department of Physics, Chemistry and Biology, Linköping University, Linköping, Sweden

Thomas Gaillard Laboratoire de Biochimie (UMR CNRS 7654), Department of Biology, Ecole Polytechnique, Palaiseau, France

Lars Goerigk School of Chemistry, The University of Sydney, Sydney, New South Wales, Australia

Hironori Hara Institute for Advanced Research and Department of Chemistry, Nagoya University, Nagoya, Japan

Jessica Hermet CEA-DAM, DIF, Arpajon, France

Genki Ichinose Department of Systems and Control Engineering, Anan National College of Technology, Anan, Tokushima, Japan

Stephan Irle Institute for Advanced Research and Department of Chemistry, Nagoya University, Nagoya, Japan

Yoshio Kato Institute for Advanced Research and Department of Chemistry, Nagoya University, Nagoya, Japan

Zhenyu Li Hefei National Laboratory for Physical Sciences at Microscale, University of Science and Technology of China, Hefei, Anhui, China

Anne Lopes Laboratoire de Biochimie (UMR CNRS 7654), Department of Biology, Ecole Polytechnique, Palaiseau, France

Ning Lu Hefei National Laboratory for Physical Sciences at Microscale, University of Science and Technology of China, Hefei, Anhui, China

David Mignon Laboratoire de Biochimie (UMR CNRS 7654), Department of Biology, Ecole Polytechnique, Palaiseau, France

Thomas A. Niehaus Department of Theoretical Physics, University of Regensburg, Regensburg, Germany

Jeffrey R. Reimers School of Chemistry, The University of Sydney, Sydney, New South Wales, Australia

Marcel Schmidt am Busch Laboratoire de Biochimie (UMR CNRS 7654), Department of Biology, Ecole Polytechnique, Palaiseau, France; Institut fuer theoretische Physik, Johannes Kepler Universitaet Linz, Linz, Austria

Thomas Simonson Laboratoire de Biochimie (UMR CNRS 7654), Department of Biology, Ecole Polytechnique, Palaiseau, France

Shanshan Wu College of Chemistry, Sichuan University, Chengdu, Sichuan, P.R. China

Dingguo Xu College of Chemistry, Sichuan University, Chengdu, Sichuan, P.R. China

Ying Xue College of Chemistry, Key Lab of Green Chemistry and Technology in Ministry of Education, Sichuan University, Chengdu, P.R. China

Xue-Gang Yang College of Chemistry, Key Lab of Green Chemistry and Technology in Ministry of Education, Sichuan University, Chengdu, P.R. China

Rui-Qin Zhang Department of Physics and Materials Science, City University Hong Kong, Hong Kong SAR, China

Min Zheng College of Chemistry, Sichuan University, Chengdu, Sichuan, P.R. China

Part I
Material Sciences

Chapter 1
Towards a Greater Accuracy in DFT Calculations: From GGA to Hybrid Functionals

Jessica Hermet, Carlo Adamo, and Pietro Cortona

1.1 Introduction

Most electronic structure calculations are performed in the framework of the density-functional theory (DFT) [1–3]. The need to take into account the electronic correlation and the increasing interest for very large systems, are the main reasons for that. Actually, DFT calculations are fast and sufficiently accurate for many applications. The electron correlation effects are taken into account by means of the correlation energy functional. Strictly speaking, this functional is the only quantity, which requires some approximations. The exchange interaction can be accounted for in an exact manner, but the experience has shown that it is easier to obtain good results by constructing approximations of the exchange-correlation energy than treating the exchange exactly and the correlation approximately.

There are different kinds of exchange-correlation functionals. The local and semi-local ones are the most efficient from the computational cost standpoint. They were the first ones to be used in actual calculations and they give quite accurate results for a number of properties, such as equilibrium geometries, vibration frequencies, and crystal compressibilities.

J. Hermet
CEA-DAM, DIF, 91297 Arpajon, France
e-mail: jessica.hermet@cea.fr

C. Adamo
Laboratoire d'Électrochimie, Chimie des Interfaces et Modélisation pour l'Énergie (UMR 7575), Centre National de la Recherche Scientifique, Chimie ParisTech, 11 rue P. et M. Curie, 75231 Paris Cedex 05, France
e-mail: carlo-adamo@chimie-paristech.fr

P. Cortona (✉)
Laboratoire Structure, Propriétés et Modélisation des Solides, UMR 8580, École Centrale Paris, Grande Voie des Vignes, 92295 Châtenay-Malabry, France
e-mail: pietro.cortona@ecp.fr

J. Zeng et al. (eds.), *Quantum Simulations of Materials and Biological Systems*,
DOI 10.1007/978-94-007-4948-1_1,

Local functionals are mainly represented by the various parametrization of the local-density approximation [4–6]. Among the semi-local functionals, two classes are usually distinguished: generalized-gradient approximations (GGAs) and meta-GGAs. These classes are characterized by their dependence on the density: GGAs depends on the density and on its reduced gradient; meta-GGAs contain an additional dependence on the Laplacian of the density and/or on the kinetic energy density. Highly popular examples of GGA functionals are the Perdew-Burke-Ernzerhof (PBE) [7] and the Becke-Lee-Yang-Parr (BLYP) [8, 9] ones, while the functional proposed by Tao, Perdew, Staroverov, and Scuseria [10] is a member of the meta-GGA class. A further distinction can be made between parameter-free functionals (i.e. functionals entirely determined on the basis of theoretical arguments) and empirical functionals (i.e. functionals containing parameters determined by fitting some reference datasets). PBE and TPSS are parameter-free functionals, BLYP is an empirical one.

Although the results obtained for many properties by local or semi-local functionals are satisfactory, in a number of cases these functionals fail or their results are not sufficiently accurate. This is the case, for example, of the evaluation of the energy barriers for chemical reactions, which are usually strongly underestimated. Hybrid functionals were devised in order to bypass these failures. The basic idea is to combine a local or semi-local density-functional with a fraction of the exact exchange. After the pioneering paper by Becke [11], many different ways of implementing this idea were devised. The simplest and more intuitive one consists in taking a linear combination of the Hartree-Fock (HF) exchange with an approximate exchange density-functional, according to the following formula:

$$E_{xc} = a_0 E_x^{HF} + (1 - a_0) E_x^{DFA} + E_c^{DFA}. \tag{1.1}$$

In (1.1), E_c^{DFA} is an approximate correlation density-functional and a_0 is a parameter, which can be determined by fitting some reference datasets or, possibly, by theoretical considerations. The functionals described by (1.1) are the so-called one-parameter global hybrids, which are probably best represented by the PBE0 functional [12, 13].

A more sophisticated way of mixing HF and DF exchanges is given by the range-separation procedure. The Coulomb inter-electron interaction is split in two terms:

$$\frac{1}{r} = \frac{1 - g(r)}{r} + \frac{g(r)}{r}, \tag{1.2}$$

where $g(r)$ is a function, which vanishes for $r = 0$ and is equal to 1 for $r \to \infty$. Usually, $g(r)$ is assumed to be the error function $erf(\omega r)$, mainly for computational convenience. The first term in the right member of (1.2) is the short-range term, while the second one is the long-range contribution. The idea underlying the range-separation approach is to use a local or semi-local exchange functional for the short-range part of the interaction and to treat exactly (i.e. by the HF theory) the long-range contribution. This gives rise to functionals having the expression:

$$E_{xc} = E_x^{DFA,SR}(\omega) + E_x^{HF,LR}(\omega) + E_c^{DFA}. \tag{1.3}$$

The parameter ω regulates the range-separation: for $\omega = 0$, Eq. (1.3) is a pure DFA; for $\omega = 1$, the exchange is the HF one; the intermediate values gradually change the first functional into the second one.

In order to perform actual calculations by (1.3), explicit expressions of $E_x^{DFA,SR}$ are required. Currently, there are two methods of solving this problem. The first one is due to Iikura et al. [14], and allows one to derive an expression for $E_x^{DFA,SR}$ starting from any usual exchange functional. The second one was proposed by Heyd, Scuseria, and Ernzerhof [15, 16] and can only be applied if an explicit model of the exchange hole is available.

The ideas underlying global and range-separated hybrids can be combined to give a third class of functionals: the range-separated global hybrids. Their expression can be obtained by using a global hybrid instead of a pure density-functional for the short-range contribution in (1.3) [17]:

$$E_{xc} = a_0 E_x^{HF,SR}(\omega) + (1 - a_0) E_x^{DFA,SR}(\omega) + E_x^{HF,LR}(\omega) + E_c^{DFA}. \tag{1.4}$$

An even more general expression could be obtained if the HF exchange is replaced by a global hybrid in the long-range contribution. However, the resulting three-parameter hybrid would not have the correct asymptotic behavior. For this reason, we have not considered this latter possibility in our work.

In this chapter, we describe the construction of new hybrid functionals based on the local and GGA functionals developed in our group [18–20]. All the three approaches mentioned above will be considered. The results reported in the present chapter complete those that have been recently published in Ref. [21].

1.2 The Starting Local and GGA Functionals

The hybrids that will be described in this chapter are based on four functionals: one of them is local, the other three are GGA-like. The local functional is the sum of the standard Slater exchange with the correlation functional proposed by Ragot and Cortona [18]. The latter, in its spin-polarized form, is given by:

$$E_c^{RC} = \int A\big(r_s(\mathbf{r})\big) C\big(\zeta(\mathbf{r})\big)\, d^3r, \tag{1.5}$$

where $A(r_s(\mathbf{r}))$ is the correlation energy per unit volume of unpolarized systems:

$$A\big(r_s(\mathbf{r})\big) = \frac{3}{4\pi r_s^3} \varepsilon_c^{RC}\big(r_s(\mathbf{r})\big), \tag{1.6}$$

and $C(\zeta(\mathbf{r}))$ is the Wang and Perdew [22] polarization factor:

$$C\big(\zeta(\mathbf{r})\big) = \left\{ \frac{1}{2}\Big[\big(1 + \zeta(\mathbf{r})\big)^{\frac{2}{3}} + \big(1 - \zeta(\mathbf{r})\big)^{\frac{2}{3}} \Big] \right\}^3. \tag{1.7}$$

The Ragot-Cortona correlation energy per electron ε_c^{RC} is given by [18]:

$$\varepsilon_c^{RC} = \frac{-0.655868 \arctan(4.888270 + 3.177037 r_s) + 0.897889}{r_s}. \tag{1.8}$$

It was obtained by a modified Colle-Salvetti approach. At first, an analytic expression of the kinetic contribution to the correlation energy per electron was determined. Then, the total correlation energy was derived by means of the DFT virial theorem. The value of the only parameter entering in this approach was fixed by applying the resulting expression to the uniform electron gas (UEG) in the low and high density limit cases. Thus, in spite of the constants entering in (1.8), the RC correlation functional is parameter-free.

This local functional, which hereafter will be referred to as S-RC, gives results, which are considerably better than those of the usual LDA [23, 24]. For example, the mean absolute error (MAE) for the G2 dataset (atomization energies of 148 molecules) is reduced by a factor of 3 [23].

The GGA functionals were constructed by Tognetti, Cortona, and Adamo (TCA) by including in (1.5) gradient-dependent contributions. The simplest way of doing that consists in including in the integral a third term depending only on the reduced density gradient s [19]:

$$E_c^{TCA} = \int A\big(r_s(\mathbf{r})\big)B\big(s(\mathbf{r})\big)C\big(\zeta(\mathbf{r})\big)\,d^3r, \tag{1.9}$$

where the reduced density gradient is defined by:

$$s = \frac{\|\nabla\rho\|}{2(3\pi^2)^{1/3}\rho^{4/3}}. \tag{1.10}$$

Parameter-free functionals are usually obtained by assuming that they are given by an analytical expression suggested by some known properties of the exact functional and by determining the parameters entering in such an expression by some kind of theoretical considerations. In the present case, as (1.9) is an extension of (1.5), it is natural to require that $B(s) \to 1$ when $s \to 0$. Furthermore, it is known that the correlation energy vanishes when the reduced gradient becomes very large. A very simple expression of $B(s)$ satisfying the two conditions:

$$B(0) = 1, \qquad \lim_{s\to\infty} B(s) = 0, \tag{1.11}$$

is the following:

$$B\big(s(\mathbf{r})\big) = \frac{1}{1+\sigma s(\mathbf{r})^{\alpha}}. \tag{1.12}$$

The two parameters σ and α were determined [19] by a mean gradient analysis, without fitting any dataset. The resulting values are $\sigma = 1.43$ and $\alpha = 2.30$.

The TCA correlation was combined with the PBE exchange (giving a functional which will be referred to PBE-TCA in the following) and tested on a variety of atomic and molecular properties [19, 25–29]. The results were better than those of the PBE-PBE functional and, in some cases (e.g. for hydrogen bonds) they were as accurate as those of a hybrid functional such as PBE0 [19, 29].

Further improvements can be expected if the functional is required to have some additional properties of the exact functional. For example, the one given in (1.9), as most GGA functionals, does not vanish for one-electron systems. It is possible to

construct a GGA functional having this property by including a forth factor in the integral in Eq. (1.9) [20]:

$$E_c^{RevTCA} = \int A(r_s)B(s)C(\zeta)\big[1 - D(r_s, s, \zeta)\big]\, d^3r. \tag{1.13}$$

Once more, this new functional is an extension of the previous ones. Thus, it is natural to require that, under given conditions, it reduces to the RC and TCA ones. In particular, in the homogeneous case, it should recover the RC functional. This is the case if $D(r_s, 0, \zeta) = 0$. Furthermore, the condition $D(r_s, s, 0) = 0$ makes (1.9) and (1.13) identical for non spin-polarized systems. A third condition, $-\infty < D \leq 1$, warrants that the correlation energy is negative and equal to zero when the reduced gradient tends to infinity. Finally, a correlation energy almost equal to zero for one-electron systems can be obtained by requiring that $D(r_s, s, \zeta) = 1$ for all the hydrogenoïd atoms, i.e. when:

$$\frac{s(\mathbf{r})}{r_s(\mathbf{r})} = aZ, \quad \text{with } a = \left(\frac{4}{9\pi}\right)^{\frac{1}{3}}. \tag{1.14}$$

The four conditions mentioned above can be satisfied by choosing:

$$D(r_s, s, \zeta) = \zeta^4 \left\{1 - \left[\operatorname{sinc}\left(\frac{\pi s}{a r_s}\right)\right]^2\right\}. \tag{1.15}$$

The RevTCA correlation, combined with the PBE exchange, gives a functional which will be referred to as PBE-RevTCA. The results given by this functional are not satisfactory: the MAE in the atomization energies of the G2 dataset is greater than the PBE-PBE one (20.4 and 17.0 kcal/mol, respectively), and much greater than the PBE-TCA MAE, which amounts to only 9.0 kcal/mol.

The results obtained by the RevTCA correlation can be improved by choosing another exchange functional or modifying the PBE one. The PBE exchange is given by:

$$E_x^{PBE} = \int e_x^{UEG}\big(r_s(\mathbf{r})\big) F_x^{PBE}\big(s(\mathbf{r})\big)\, d^3r, \tag{1.16}$$

where

$$F_x^{PBE}(s) = 1 + \kappa - \frac{\kappa}{1 + \frac{\mu}{\kappa} s^2}. \tag{1.17}$$

F_x^{PBE} contains two parameters, which were determined by requiring that the LDA linear response is recovered (μ), and the *local* Lieb-Oxford condition [30] is verified everywhere (κ). As it was pointed out by Zhang and Yang [31], the latter is a too strong condition, because the original Lieb-Oxford relation is an integral one. Zhang and Yang determined the value of κ by fitting a set of atomization energies. Tognetti et al. preferred to choose κ so that the local Lieb-Oxford condition, as improved by Chan and Handy [32], is verified just in the so-called *physical interval*, i.e. for $s \in [0\text{–}3]$. In such a way they found $\kappa = 1.227$, a value quite different from the original PBE one ($\kappa = 0.804$).

The modified PBE exchange (ModPBE), obtained assuming $\kappa = 1.227$ in (1.17), was combined with the RevTCA correlation. The resulting ModPBE-RevTCA functional gave excellent results for properties such as atomization energies and barrier heights for chemical reactions. For example, the MAE in the atomization energies of the G2 dataset amounts to only 5.9 kcal/mol, a value almost 3 times smaller than the PBE-PBE one, and quite close to the PBE0 MAE (5.0 kcal/mol). However, the tests of this functional showed also some failures: for example, the PBE-TCA description of the hydrogen bonds is fairly more accurate.

1.3 Technical Details

All the calculations were performed self-consistently with a locally modified version of the Gaussian-03 code [33], using the 6-311 + G(3df, 2p) basis set. We have optimized the a_0 and/or ω values by evaluating the performances of the functionals for several properties, including atomization energies, reaction barrier heights, and binding energies of noncovalently bound systems.

For atomization energies, we used the standard reference set G2-148 compiled by Curtiss et al. [34], listing experimental data of 148 molecules, compounded of first- and second-row elements.

A benchmark set of barrier heights of hydrogen transfer, heavy-atom transfer (i.e. transfer of atoms other than H), nucleophilic substitution, unimolecular and association reactions, was recently assembled by Truhlar and coworkers [35, 36]. It consists of forward and reverse barrier heights for 12 reactions and will be referred to as DBH24. The best estimates of the barrier heights, as well as the geometries of all the species in this set, optimized with a correlated wave function method, are available in the supporting information of Ref. [36].

To complete the test panel, noncovalent interactions of 31 complexes were considered. These complexes were retained by Zhao and Truhlar for their NCB31 dataset [37, 38], and are representative of systems characterized by hydrogen bonds, charge transfer, dipole interaction, weak interaction, and π–π stacking. All geometries and best estimates for the binding energies, calculated by the Weizmann (W1) theory, are available in the Truhlar group website.

1.4 Hybrid Functionals

We start our discussion of the hybrid functionals with the global hybrids. The atomization energies, barrier heights, and noncovalent binding energies for the systems belonging to the G2, DBH24, and NCB31 datasets have been calculated in function of a_0. The resulting MAEs are reported in Figs. 1.1, 1.2, and 1.3.

Considering at first the barrier heights (Fig. 1.1), it is seen that the four functionals have a quite similar behavior. All the curves have a pronounced minimum for

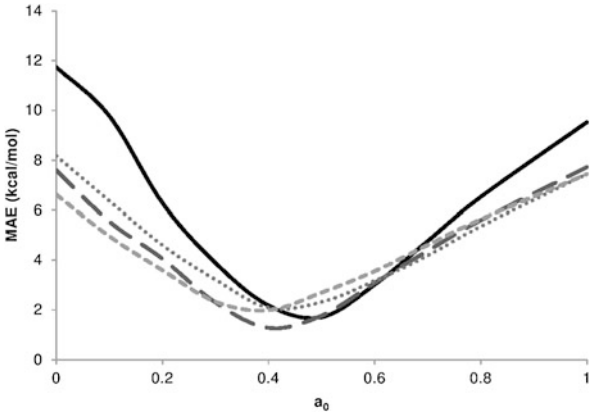

Fig. 1.1 MAEs in the barrier heights of the DBH24 dataset (in kcal/mol) of the global hybrids based on the S-RC, PBE-TCA, PBE-RevTCA, and ModPBE-RevTCA functionals. The results are given in function of the mixing parameter a_0. *Full line*: S-RC. *Long-dashed line*: PBE-TCA. *Dotted line*: PBE-RevTCA. *Short-dashed line*: ModPBE-RevTCA

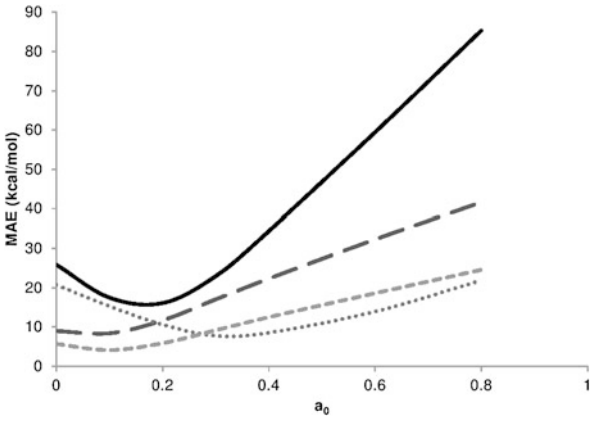

Fig. 1.2 MAEs in the atomization energies of the G2 dataset (in kcal/mol) of the global hybrids based on the S-RC, PBE-TCA, PBE-RevTCA, and ModPBE-RevTCA functionals. The results are given in function of the mixing parameter a_0. *Full line*: S-RC. *Long-dashed line*: PBE-TCA. *Dotted line*: PBE-RevTCA. *Short-dashed line*: ModPBE-RevTCA

a_0 values within the interval [0.3–0.5], the corresponding MAEs being between 1.2 and 2.1 kcal/mol.

The results for the atomization energies, reported in Fig. 1.2, have a quite different trend. Two functionals, PBE-TCA and ModPBE-RevTCA take only a modest advantage from the hybridization process. On the contrary, the PBE-RevTCA MAE is considerably reduced and takes a minimum value around $a_0 = 1/3$. The S-RC curve also presents a pronounced minimum near to $a_0 = 0.2$, but the corresponding MAE (16.1 kcal/mol) is too large for a hybrid functional, considering the additional computational cost due to the HF contribution.

Figure 1.3, where the MAEs in noncovalent binding energies are reported, displays still different features. Quite surprisingly, the best results are the S-RC ones: for $a_0 = 0.6$ the MAE is only 0.44 kcal/mol. PBE-TCA and PBE-RevTCA are the same approximation for these closed-shell systems. Starting from $a_0 = 0.3$, their MAE remains approximately constant, taking values close to 0.7 kcal/mol. Finally, the ModPBE exchange is not adequate for weak interacting systems: the best results are obtained when it is completely replaced by the HF exchange, i.e. for $a_0 = 1$.

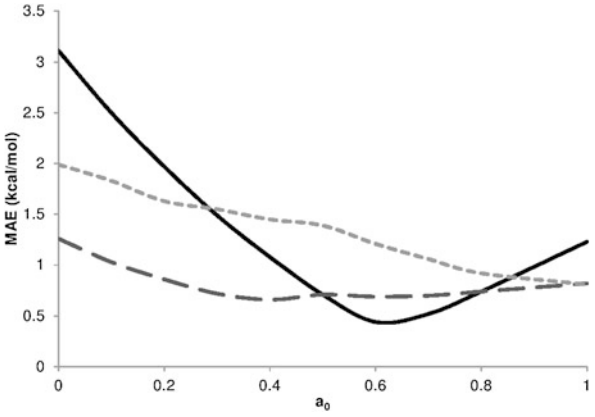

Fig. 1.3 MAEs in the noncovalent binding energies of the NCB31 dataset (in kcal/mol) of the global hybrids based on the S-RC, PBE-TCA, PBE-RevTCA, and ModPBE-RevTCA functionals. The results are given in function of the mixing parameter a_0. *Full line*: S-RC. *Long-dashed line*: PBE-TCA and PBE-RevTCA. *Short-dashed line*: ModPBE-RevTCA

The comparison of the three figures makes evident the main obstacle one meets in constructing hybrid functionals: it is difficult to find a parameter value giving good results for all the properties. In the present case, only the hybrid based on PBE-RevTCA is optimized simultaneously for the three datasets by a value of a_0 close to 0.4. In the other cases, one must choose a compromise value of a_0 or the property to be optimized. The parameter values that we consider the best for each functional are reported in Table 1.1 as well as the corresponding MAEs we have found for the three reference datasets.

The discussion of the range-separated hybrids is similar. The four functionals have a similar behavior for the barriers heights, their MAEs having a deep minimum (around 3.5 kcal/mol) for ω values in the interval [0.3–0.5] (Fig. 1.4).

This situation changes drastically when one considers the atomization energies (Fig. 1.5). The S-RC hybrid has a minimum MAE for ω close to 0.2 but, as in the case of the global hybrid, the corresponding MAE is too high. Small values of ω give rise to increasing errors of the three GGA-based hybrids. However, the errors decrease for larger ω values and a minimum is found around $\omega = 0.5$ for PBE-TCA and close to $\omega = 0.8$ for the other two hybrids. In the case of ModPBE-RevTCA, however, the minimum MAE is found for $\omega = 0$, i.e. this functional takes no advantage from the hybridization according to the range-separation procedure.

Table 1.1 MAEs (in kcal/mol) in atomization energies, barrier heights, and noncovalent binding energies of the global hybrids based on various local or semi-local functionals. The value of the mixing parameter a_0 for each case is also reported. The MAEs of the original local or semi-local functionals are given in parenthesis

	S-RC	PBE-TCA	PBE-RevTCA	ModPBE-RevTCA
a_0	0.2	0.1	0.4	0.2
G2	16.1 (26.2)	8.4 (9.0)	8.6 (20.7)	5.9 (5.9)
DBH24	6.3 (11.8)	5.6 (7.6)	2.1 (8.2)	3.6 (6.6)
NCB31	2.0 (3.1)	1.0 (1.3)	0.7 (1.3)	1.6 (2.0)

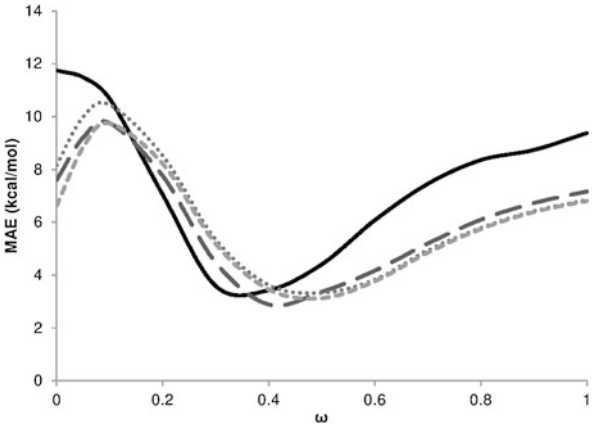

Fig. 1.4 MAEs in the barrier heights of the DBH24 dataset (in kcal/mol) of the range-separated hybrids based on the S-RC, PBE-TCA, PBE-RevTCA, and ModPBE-RevTCA functionals. The results are given in function of the range-separation parameter ω. *Full line*: S-RC. *Long-dashed line*: PBE-TCA. *Dotted line*: PBE-RevTCA. *Short-dashed line*: ModPBE-RevTCA

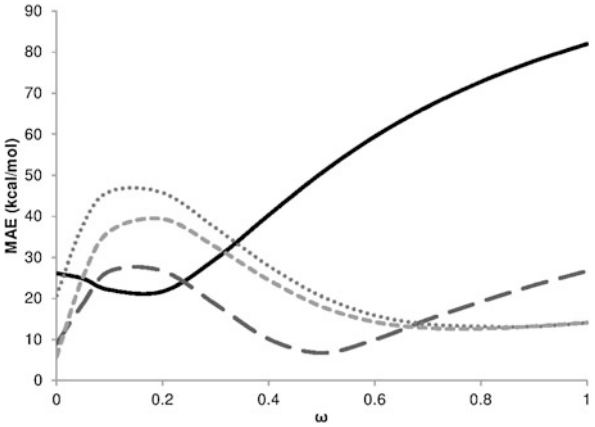

Fig. 1.5 MAEs in the atomization energies of the G2 dataset (in kcal/mol) of the range-separated hybrids based on the S-RC, PBE-TCA, PBE-RevTCA, and ModPBE-RevTCA functionals. The results are given in function of the range-separation parameter ω. *Full line*: S-RC. *Long-dashed line*: PBE-TCA. *Dotted line*: PBE-RevTCA. *Short-dashed line*: ModPBE-RevTCA

The MAEs in the noncovalent binding energies are reported in Fig. 1.6. It appears that, for $\omega > 0.5$ the DFT exchange have no longer a role: the three GGA-based hybrids, which share the same correlation functional for closed-shells systems, give practically the same results. All the functionals have a minimum MAE for ω values not far from those which minimize the errors for the DBH24 dataset.

As in the case of the global hybrids, the final ω values for the various functionals are determined by the need of finding a compromise between the value which optimize the barriers heights and the noncovalent binding energies on one hand, and the atomization energies on the other hand. Once more, only one functional (the one based on PBE-TCA, in the present case) is optimized by approximately the same value of ω for the three dataset. In Table 1.2, the ω values we have chosen are reported, as well as the resulting MAEs of the four functionals for the three datasets.

Finally, we consider the range-separated global hybrids. In this case, there are two parameters to be optimized, a_0 and ω. The results we have obtained by the hybrid based on the PBE-TCA functional are shown in Figs. 1.7, 1.8, and 1.9. In

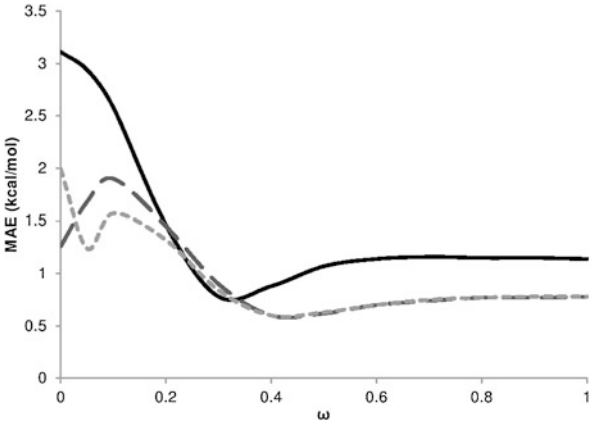

Fig. 1.6 MAEs in the noncovalent binding energies of the NCB31 dataset (in kcal/mol) of the range-separated hybrids based on the S-RC, PBE-TCA, PBE-RevTCA, and ModPBE-RevTCA functionals. The results are given in function of the range-separation parameter ω. *Full line*: S-RC. *Long-dashed line*: PBE-TCA and PBE-RevTCA. *Short-dashed line*: ModPBE-RevTCA

these figures, the MAE is plotted in function of ω for various values of the mixing parameter a_0.

Considering, at first, the atomization energies (Fig. 1.7), it can be seen that the functional changes its behavior in the interval [0–0.4] with the increase of the a_0 value. The maximum displayed by the pure range-separated functional curve ($a_0 = 0$) becomes progressively less pronounced. It is replaced by a flat region for $a_0 = 0.3$ and by a minimum for greater values of a_0. For $a_0 = 0.2$ and $a_0 = 0.25$, the curves present two minima. The one at smaller ω value corresponds to a smaller MAE, but the second one is more interesting when the other datasets are considered.

The MAEs in barrier heights are reported in Fig. 1.8. The minimum error is obtained by the global hybrid with $a_0 = 0.4$. However, the MAE in atomization energies of such functional is too large. Much more interesting are the results obtained with $a_0 = 0.2$ or $a_0 = 0.25$, which display a minimum simultaneously for the atomization energies and the barrier heights. In particular, the range-separated global hybrid with $a_0 = 0.25$ and $\omega = 0.3$ is the one which gives the best accuracy. This conclusion is confirmed by the results for the noncovalent binding energies, reported in Fig. 1.9. The MAEs of this hybrid, i.e. the one with $a_0 = 0.25$ and $\omega = 0.3$, are 5.9, 2.5, and 0.6 kcal/mol for the G2, DBH24, and NCB31 datasets, respectively.

Table 1.2 MAEs (in kcal/mol) in atomization energies, barrier heights, and noncovalent binding energies of the range-separated hybrids based on various local or semi-local functionals. The value of the range-separation parameter ω for each case is also reported. The MAEs of the original local or semi-local functionals are given in parenthesis

	S-RC	PBE-TCA	PBE-RevTCA	ModPBE-RevTCA
ω	0.3	0.5	0.7	0.0
G2	29.7 (26.2)	6.8 (9.0)	13.7 (20.7)	5.9
DBH24	3.6 (11.8)	3.4 (7.6)	4.9 (8.2)	6.6
NCB31	0.8 (3.1)	0.6 (1.3)	0.8 (1.3)	2.0